Supplementary Information

Free-Energy Barriers and Reaction Mechanisms for the Electrochemical Reduction of CO on the Cu(100) Surface, Including Multiple Layers of Explicit Solvent at pH 0

Tao Cheng, Hai Xiao and William A. Goddard III*

Materials and Process Simulation Center,

California Institute of Technology, Pasadena, CA 91125, U. S. A.

*Corresponding author E-mail: wag@wag.caltech.edu

S1. Simulation Methods

Electronic structure calculations were performed within the framework of DFT, as implemented in the Vienna ab initio simulation program (VASP),[1-4] a plane-wave pseudopotential package. The exchange and correlation energies were calculated using the Perdew, Burke, and Ernzerhof (PBE) functional within the generalized gradient approximation (GGA). [5-6] A plane-wave cutoff energy of 400 eV was used. The First order Methfessel-Paxton scheme was used with a smearing width of 0.2 ev. Dipole corrections were applied along the z axis. The PBE-D3 method was employed to correct van der Waals interaction of water-water and water-Cu.[7] The Energy minimization criterion was that all forces on free atoms are < 0.01 eV/Å. The charges on species were derived using a Bader analysis.[8-9] An implicit solvation model, Vaspsol,[10-11] was used to describe the effect of electrostatics, cavitation, and dispersion on the interaction between a solute and solvent as implemented in VASP.

A 1.2 fs time step with used In the Molecular Dynamics (MD) simulations with hydrogen mass set to 2. These MD simulations used only the gamma point of the Brillouin zone with no consideration of symmetry. The velocities were rescaled every 20 MD steps to readjust to the target temperature in equilibration. A Nose Hoover thermostat was employed for the free energy calculations with a temperature damping parameter of 100 fs.

The calculations used a 3 layer Cu(100) metal slab, based on a 4 × 4 periodic cell with the bottom two layers fixed. The water slab contains 49 water molecules placed on the Cu(100) surface to explicitly simulate the water/Cu(100) interface. The thickness of the water slab is about 12 Å corresponding to 5 layers of water. The simulation box is 50 Å along the z axis with a vacuum of 34 Å. The lateral dimensions of the slab were fixed using a 3.61 Å lattice constant. Two CO molecules were placed on the 4 × 4 unit cell (on top site) corresponding to a surface coverage of 1/8 ML.

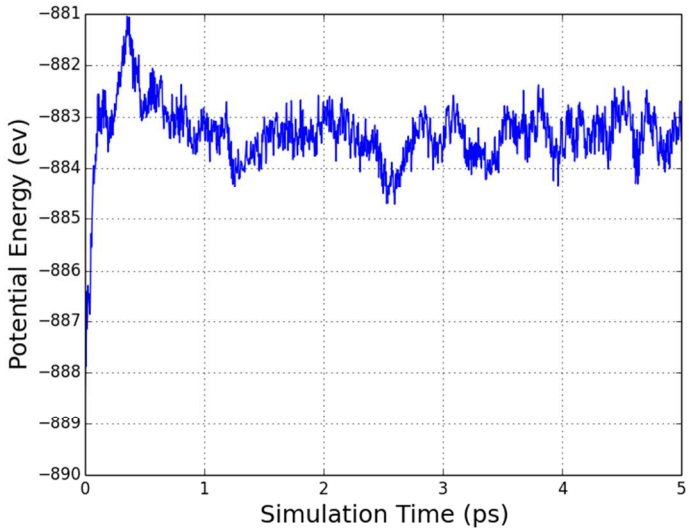

Figure S1. Potential energy over 5ps QMD simulation at 198K for the water/Cu(100) interface.

S2. Metadynamics

The metadynamics Hamiltonian $\widetilde{H}(p,q,t)$ is written as[12]:

$$\widetilde{H}(p,q,t) = H(p,q) + \tilde{V}(t,\xi), \tag{S1}$$

where *H(p,q)* is the Hamiltonian for the original (unbiased) system, ξ is the collective variable (**CV**), and $\tilde{V}(t,\xi)$ is the time-dependent bias potential. The bias term is defined as a sum of Gaussian hills with **height *h*** and **width *ω***:

$$\tilde{V}(t,\xi) = h\sum_{i=1}^{|t/t_G|} \exp[-\frac{|\xi^{(t)}-\xi^{(i\cdot t_G)}|^2}{2\omega}], \tag{S2}$$

The biased potential is related to the free energy via:

$$A(\xi) = \lim_{t\to\infty} \tilde{V}(t,\xi) + const \tag{S3}$$

Three parameters are controllable and relevant to the accuracy in a metadynamics simulation: height of a Gaussian hill (h), width of the Gaussian hill (ω) and frequency to update the bias potential (t_G). In this work, we based the parameters tests for an ideal double well model with a transition barrier of 0.6 ev. We found the best set of parameters balancing both accuracy and efficiency is as following:

- h = 0.08 ev
- ω = 0.18 Å
- t_G = 20 time step

the Metadynamics simulations were continued until the first barrier crossing. This also applies for the reverse processes. Two or three independent simulations were carried out for each case to improve accuracy and the statists.

S3. Constrained Molecular dynamics[13]

The correct (*unbiased*) average for a quantity $\alpha(\xi)$ of constrained (*biased*) molecular dynamicsis given by (S4):

$$\alpha(\xi) = \frac{\left\langle |\boldsymbol{Z}|^{-\frac{1}{2}}\alpha(\xi^*)\right\rangle_{\xi^*}}{\left\langle |\boldsymbol{Z}|^{-\frac{1}{2}}\right\rangle_{\xi^*}} \tag{S4}$$

where Z is a mass metric tensor defined as:

$$\boldsymbol{Z}_{\alpha,\beta} = \sum_{i=1}^{3N} m_i^{-1}\nabla_i\xi_\alpha \cdot \nabla_i\xi_\beta \tag{S5}$$

The free energy gradient can be computed using the equation: [13]

$$\left(\frac{\partial A}{\partial \xi_k}\right)_{\xi^*} = \frac{1}{\left\langle |\boldsymbol{Z}|^{-\frac{1}{2}}\right\rangle_{\xi^*}} \left\langle |\boldsymbol{Z}|^{-\frac{1}{2}}\left[\lambda_k + \frac{k_B T}{2|\boldsymbol{Z}|}\sum_{j=1}^{r}(\boldsymbol{Z}^{-1})_{k_j}\sum_{i=1}^{3N} m_i^{-1}\nabla_i\xi_j \cdot \nabla_i|\boldsymbol{Z}|\right]\right\rangle_{\xi^*} \tag{S6}$$

The free-energy difference between states (1) and (2) can be computed by integrating the

free-energy gradients over a connecting path:

$$\Delta A_{1\to 2} = \int_{\xi(1)}^{\xi(2)} \left(\frac{\partial A}{\partial \xi}\right)_{\xi} \cdot d\xi \quad \text{(S7)}$$

We first employed slow-growth to generate the reaction path. We applied an increment of 0.0008 Å/step to collective variables to drive the chemical reactions. We found that simulation times of 2 to 10 ps were necessary to complete the reaction, depending on the length of reaction pathways. From the reactive trajectories, we selected twenty (21) windows for thermodynamic integration calculations. Simulations of 2.4 ps were carried out at each window to produce the potential of mean force (PMF). Free energy profiles were obtained by integrating the PMF.

S4. Collective Variables

For Langmuir-Hinshelwood reactions, the distance ($R_{C\text{-}H,}$in Å) between surface hydrogen (H*) and carbon (C) or the distance ($R_{O\text{-}H,}$in Å) between surface hydrogen (H*) and Oxygen (O) of CH_xO were used as collective variables.

For the proton transfer reactions (Eley-Rideal reactions), the collective variables ($\boldsymbol{\xi}$) were defined as the square root of the summation of O-H distances connecting the hydrogen bond network from H_3O^+ and to reactants (CH_xO) as following:

$$\boldsymbol{\xi} = \sqrt{\sum_{i=1}^{n_{water}} \boldsymbol{r}_{O_{i+1}-H_i}{}^2} \quad \text{(S8)}$$

Here $r_{O_{i+1}-H_i}$ is the distance between oxygen and hydrogen (Figure S2). n_{water} is the number of water involved in the H-Bond network.

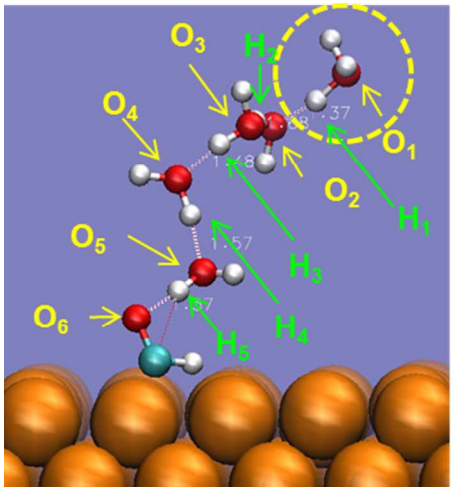

Figure S2. The HB network connecting H_3O^+ and CHO* for reaction R2a

Table S1. The collective variables defined for each reduction reaction.

H(N)	Reactions	Collective variables (Å)
1a	$CO^* + H^* \rightarrow CHO^*$	$R_{C\text{-}H}$[c]
1b	$CO^* + H^* \rightarrow COH^*$	$R_{O\text{-}H}$[a]
1c	$CO^* + H_3O^+ + e^- \rightarrow COH^* + H_2O(aq)$	$H_3O^+(nH_2O)$-O[b]
1d	$CO^* + H_2O^* \rightarrow COH^* + OH^*$	$R_{O\text{-}H}$[a]
2a	$CHO^* + (H_3O)^+ + e^- \rightarrow CHOH^*$	$H_3O^+(nH_2O)$-O[b]
2b	$CHO^* + H_2O^* \rightarrow CHOH^* + OH^*$	$H_2O(nH_2O)$-O[b]
2c	$CHO^* + H^* \rightarrow CH_2O^*$	$R_{C\text{-}H}$[c]
3a‡	$CHOH^* + (H_3O)^+ + e^- \rightarrow CH^* + H_2O(aq)$	$H_3O^+(nH_2O)$-O[b] $R_{C\text{-}H}$[c]
3b	$CHOH^* + (H_3O)^+ + e^- \rightarrow CH \cdots H_2O^*$	$H_3O^+(nH_2O)$-O[b]
3b^{dehydration}	$CH \cdots H_2O^* \rightarrow CH^* + H_2O^*(aq)$	$R_{C\text{-}O}$[d]
3c	$CHOH^* + H^* \rightarrow CH_2OH^*$	$R_{C\text{-}H}$[c]
4a	$CH^* + H^* \rightarrow CH_2^*$	$R_{C\text{-}H}$[c]
4b	$CH_2OH + H^* \rightarrow CH_3OH^*$	$R_{C\text{-}H}$[c]
5	$CH_2^* + H^* \rightarrow CH_3^*$	$R_{C\text{-}H}$[c]
6	$CH_3^* + H^* \rightarrow CH_4^*$	$R_{C\text{-}H}$[c]

[a] The distance between O(H_xCO) and H*

[b] The distance between C and H*

[c] H-Bond network as defined in equation S8

[d] The distance between C and O

‡ Two dimension metadynamics simulation.

S5. Free energy calculations

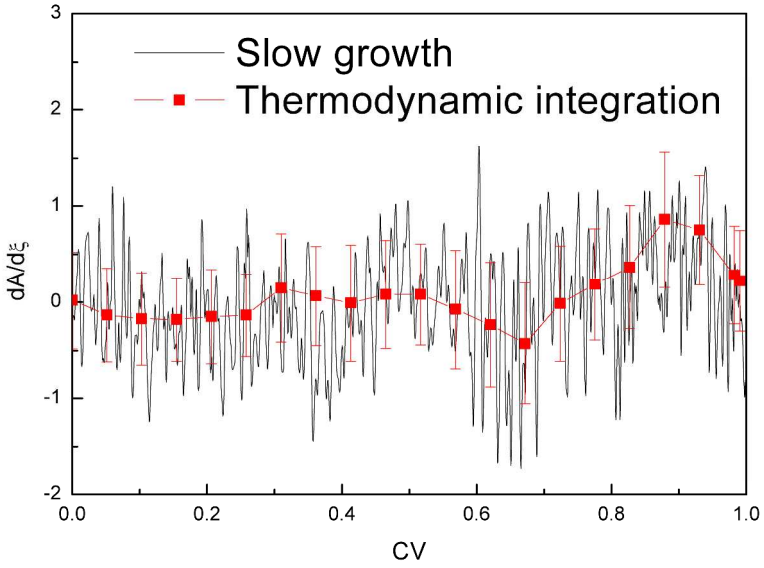

Figure S3. Potential of mean force ($\frac{\partial A}{\partial \xi}$) derived from slow growth simulation (black) and thermodynamic inteagration (TI, red) of reaction R2a in Table S1 ($CHO^* + (H_3O)^+ + e^- \rightarrow CHOH^*$).

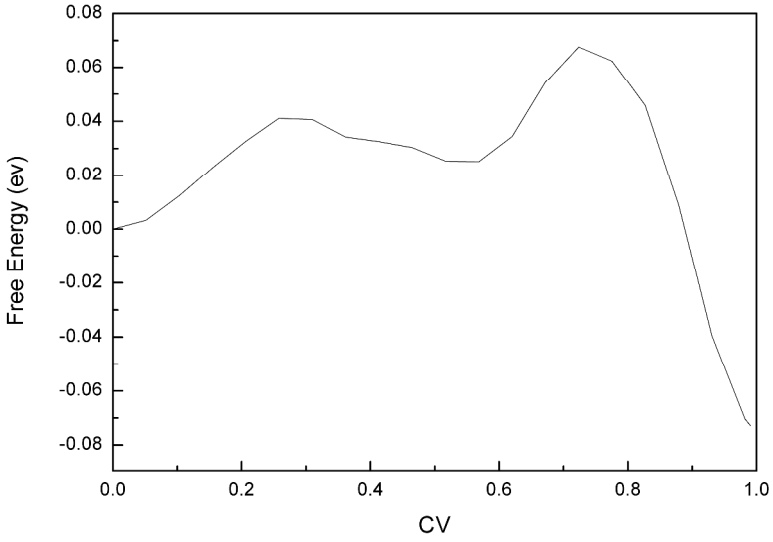

Figure S4. The free energy profiles along the collective barriers of reaction 2a in Table S1 ($CHO^* + (H_3O)^+ + e^- \rightarrow CHOH^*$), which is derived from integrating the PMF from the TI calculations in Figure S3.

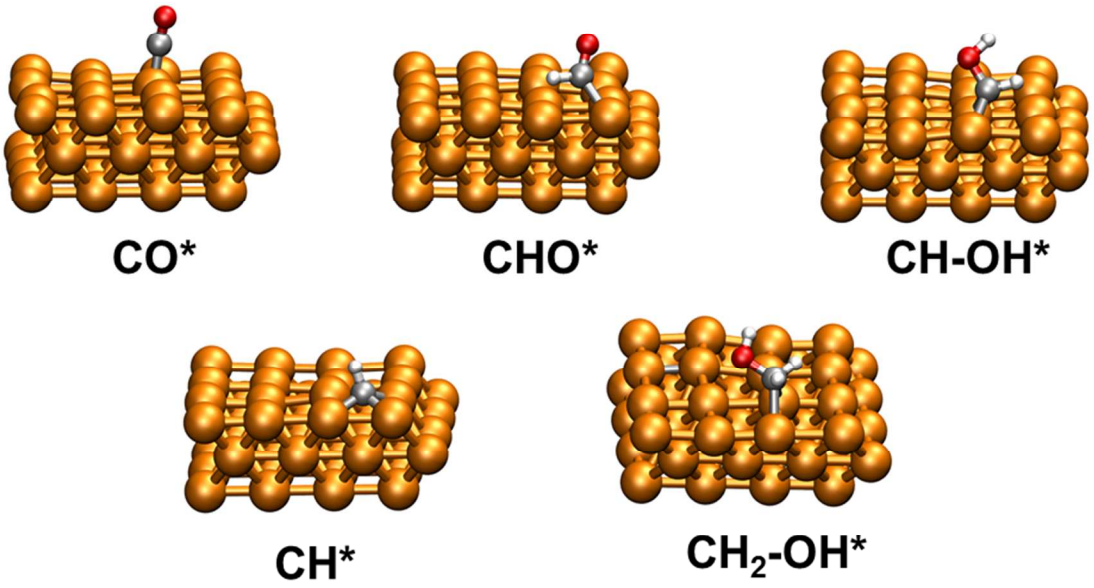

Figure S5. The species in the simulation: CO*, CHO*, CHOH*, CH* and CH_2OH*.

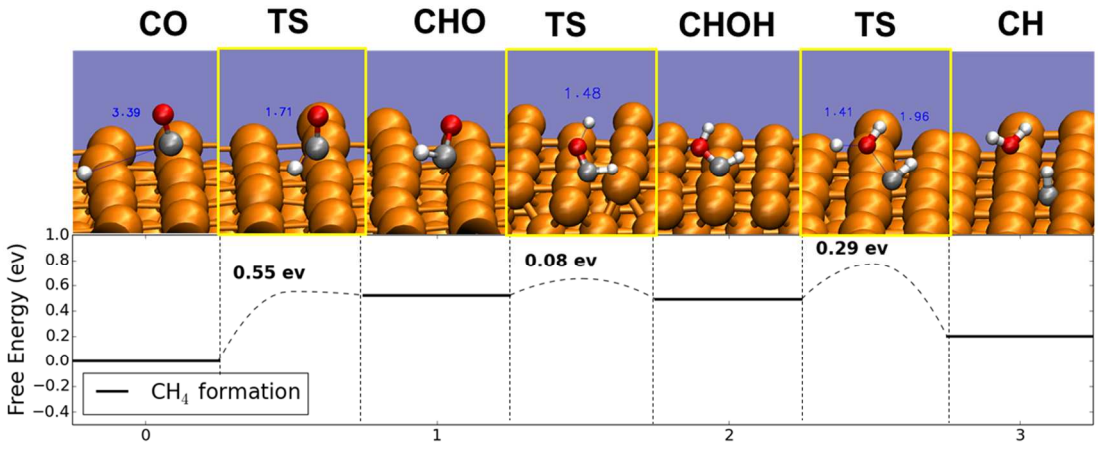

Figure S6. Free energies and configurations along with the CH_4 formation path. Reactions after CH* are ignored.

S6. Constant potential corrections

Electrochemical reaction energetics at constant potential were determined using the energy differences ($\Delta E_{\phi_1-\phi_2}$) between the initial work function (ϕ_1) and final work function (ϕ_2) using the correction proposed by Chan et al:[14]

$$\Delta E_{\phi_1-\phi_2} = E(\phi_1) - E(\phi_2) = \frac{(q_2-q_1)(\phi_2-\phi_1)}{2} \quad \text{(S8)}$$

Here, q_1, and q_2 are the charges under starting work function (ϕ_1) and end work function (ϕ_2), which based on the Bader analysis. The final extrapolated $\Delta E_{\phi_1-\phi_2}$ are shown in Table S2. These corrections were applied only to the proton transfer reactions (2a and 3a in Table S1). We did not correct the surface reactions, because the charge transfers in these reactions are too small to be significant.

Table S2. Tabulated Changes in work function from final state to initial state ($\phi_{FS} - \phi_{IS}$) and transition state to initial state ($\phi_{TS} - \phi_{IS}$), changes in charges from final state to initial state ($q_{FS} - q_{IS}$), and transition state to initial state ($q_{TS} - q_{IS}$), and resultant extrapolated energy differences ΔE_{FS-IS} and ΔE_{TS-IS}. After applying these corrections to the proton transfer reactions (2a and 3a in Table S1), all calculated free energies are under a working condition of about -0.4 V compared with SHE (4.44 V).

Reactions	$\phi_{FS} - \phi_{IS}$	$q_{FS} - q_{IS}$	$\phi_{TS} - \phi_{IS}$	$q_{TS} - q_{IS}$	ΔE_{FS-IS}	ΔE_{TS-IS}
2a	0.498	-0.227	0.495	-0.220	-0.057	-0.056
3a	0.541	-0.322	0.491	-0.292	-0.087	-0.079
HER	0.240	-0.759	0.308	-0.849	-0.100	-0.117

S7. Comparison of reaction energies of CH_4 formation

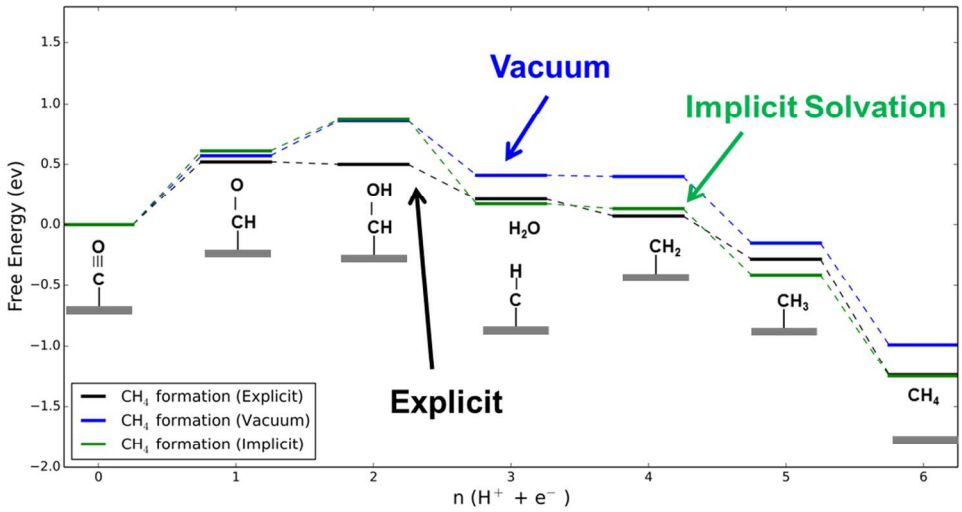

Figure S7. Comparison of reaction energies in CH_4 formation paths among Vacuum calculations, implicit solvation calculations (VASPsol) and explicit solvent calculations.

Figure S7 shows the comparison of the reaction energies among vacuum calculations, implicit solvation calculations (Vaspsol[10-11]) and explicit calculations. The results show that QM calculation with solvation model can produce the tendency of the potential map obtained from explicit calculation, but not the exact values. Large differences appear, if the species have OH group. Despite these discrepancies, QM calculations with solvation calculations are still a powerful approach, if considering the efficiency, especially for screening in large scale. Also, incorporating several explicit water moles with solvation model should increase the accuracy in principle.

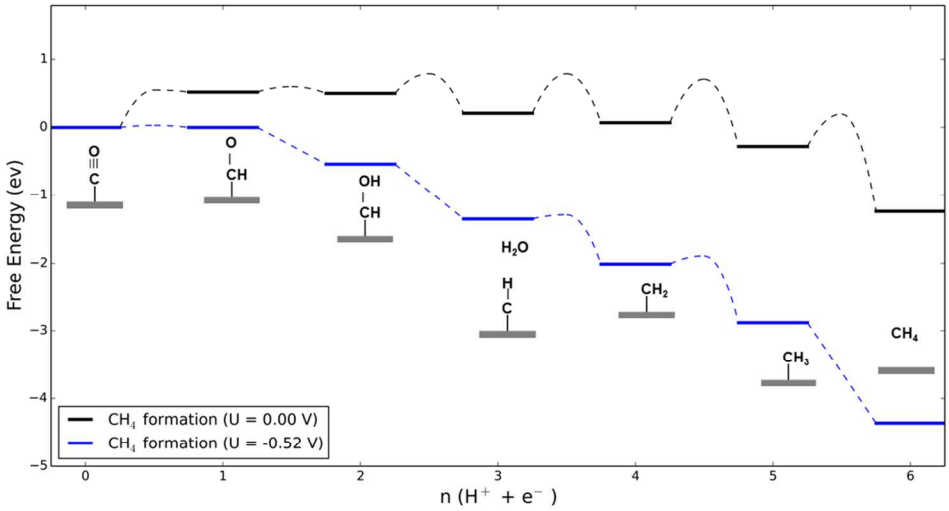

Figure S8. Lowest energy pathways for the electro-reduction of CO to methane under U = 0.0 V and U = -0.52 V. The contribution of external potential is estimated using a computational hydrogen electrode (CHE) mode.[15]

Reference

(1) Kresse, G.; Hafner, J. Ab Initio Molecular Dynamics for Liquid Metals. *Phys. Rev. B* **1993,** *47*, 558-561.

(2) Kresse, G.; Hafner, J. Ab Initio Molecular-dynamics Simulation of the Liquid-meta Amorphous-semiconductor Transition in Germanium. *Phys. Rev. B* **1994,** *49*, 14251-14269.

(3) Kresse, G.; Furthmüller, J. Efficiency of Ab-initio Total Energy Calculations for Metals and Semiconductors Using a Plane-wave Basis Set. *Comput. Mater. Sci.* **1996,** *6*, 15-50.

(4) Kresse, G.; Furthmüller, J. Efficient Iterative Schemes for Ab Initio Total-energy Calculations Using a Plane-wave Basis Set. *Phys. Rev. B* **1996,** *54*, 11169-11186.

(5) Perdew, J. P.; Chevary, J. A.; Vosko, S. H.; Jackson, K. A.; Pederson, M. R.; Singh, D. J.; Fiolhais, C. Atoms, Molecules, Solids, and Surfaces: Applications of the Generalized Gradient Approximation for Exchange and Correlation. *Phys. Rev. B* **1992,** *46*, 6671-6687.

(6) Perdew, J. P.; Chevary, J. A.; Vosko, S. H.; Jackson, K. A.; Pederson, M. R.; Singh, D. J.; Fiolhais, C. Erratum: Atoms, Molecules, Solids, and Surfaces: Applications of the Generalized Gradient Approximation for Exchange and Correlation. *Phys. Rev. B* **1993,** *48*, 4978-4978.

(7) Grimme, S.; Antony, J.; Ehrlich, S.; Krieg, H. A Consistent and Accurate Ab Initio Parametrization of Density Functional Dispersion Correction (DFT-d) for the 94 Elements H-pu. *J. Chem. Phys* **2010,** *132*, 154104.

(8) Bader, R. F. W. A Quantum Theory of Molecular Structure and Its Applications. *Chem. Rev.* **1991,** *91*, 893-928.

(9) Henkelman, G.; Arnaldsson, A.; Jónsson, H. A fast and robust algorithm for Bader decomposition of charge density. *Comput. Mater. Sci.* **2006,** *36*, 354-360.

(10) Fishman, M.; Zhuang, H. L.; Mathew, K.; Dirschka, W.; Hennig, R. G. Accuracy of Exchange-correlation Functionals and Effect of Solvation on the Surface Energy of Copper. *Phys. Rev. B* **2013,** *87*, 245402.

(11) Mathew, K.; Sundararaman, R.; Letchworth-Weaver, K.; Arias, T. A.; Hennig, R. G. Implicit Solvation Model for Density-functional Study of Nanocrystal Surfaces and Reaction Pathways. *J. Chem. Phys* **2014,** *140*, 084106.

(12) Laio, A.; Parrinello, M. Escaping Free-energy Minima. *Proc. Natl. Acad. Sci.* **2002,** *99*, 12562-12566.

(13) Fleurat-Lessard, P.; Ziegler, T. Tracing the Minimum-energy Path on the Free-energy Surface. *J. Chem. Phys* **2005,** *123*, 084101.

(14) Chan, K.; Nørskov, J. K. Electrochemical Barriers Made Simple. *J. Phys. Chem. Lett.* **2015,** *6*, 2663-2668.

(15) Peterson, A. A.; Abild-Pedersen, F.; Studt, F.; Rossmeisl, J.; Norskov, J. K. How Copper Catalyzes the Electroreduction of Carbon Dioxide into Hydrocarbon Fuels. *Energy. Environ. Sci.* **2010,** *3*, 1311-1315.